JACS
JOURNAL OF THE AMERICAN CHEMICAL SOCIETY
Article
pubs.acs.org/JACS

Coordination and Metalation Bifunctionality of Cu with 5,10,15,20-Tetra(4-pyridyl)porphyrin: Toward a Mixed-Valence Two-Dimensional Coordination Network

Yang Li,[†] Jie Xiao,[‡] Tatyana E. Shubina,[§] Min Chen,[‡] Ziliang Shi,[†] Martin Schmid,[‡] Hans-Peter Steinrück,[‡] J. Michael Gottfried,*[,‡,∥] and Nian Lin*[,†]

[†]Department of Physics, The Hong Kong University of Science and Technology, Clear Water Bay, Kowloon, Hong Kong, China
[‡]Lehrstuhl für Physikalische Chemie II, Universität Erlangen-Nürnberg, Egerlandstrasse 3, 91058 Erlangen, Germany
[§]Computer-Chemie-Centrum, Universität Erlangen-Nürnberg, Nägelsbachstrasse 25, 91052 Erlangen, Germany
[∥]Fachbereich Chemie, Philipps-Universität Marburg, Hans-Meerwein-Strasse, 35032 Marburg, Germany

Supporting Information

ABSTRACT: We investigated the coordination self-assembly and metalation reaction of Cu with 5,10,15,20-tetra(4-pyridyl)porphyrin (2HTPyP) on a Au(111) surface by means of scanning tunneling microscopy, X-ray photoelectron spectroscopy, and density functional theory calculations. 2HTPyP was found to interact with Cu through both the peripheral pyridyl groups and the porphyrin core. Pairs of pyridyl groups from neighboring molecules coordinate Cu(0) atoms, which leads to the formation of a supramolecular metal−organic coordination network. The network formation occurs at room temperature; annealing at 450 K enhances the process. The interaction of Cu with the porphyrin core is more complex. At room temperature, formation of an initial complex Cu(0)−2HTPyP is observed. Annealing at 450 K activates an intramolecular redox reaction, by which the coordinated Cu(0) is oxidized to Cu(II) and the complex Cu(II)TPyP is formed. The coordination network consists then of Cu(II) complexes linked by Cu(0) atoms; that is, it represents a mixed-valence two-dimensional coordination network consisting of an ordered array of Cu(II) and Cu(0) centers. Above 520 K, the network degrades and the Cu atoms in the linking positions diffuse into the substrate, while the Cu(II)TPyP complexes form a close-packed structure that is stabilized by weak intermolecular interactions. Density functional theory investigations show that the reaction with Cu(0) proceeds via formation of an initial complex between metal atom and porphyrin followed by formation of Cu(II) porphyrin within the course of the reaction. The activation barrier of the rate limiting step was found to be 24−37 kcal mol^{-1} depending on the method used. In addition, linear coordination of a Cu atom by two CuTPyP molecules is favorable according to gas-phase calculations.

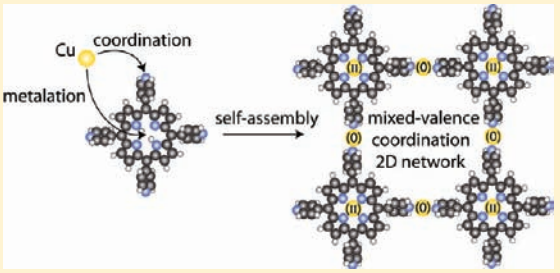

1. INTRODUCTION

Supramolecular coordination self-assembled structures have been intensively studied in past decades owing to their promising applications in catalysis, solid sensors, separations, magnetism, and storage.[1] In the past decade, self-assembly on surfaces by supramolecular coordination has provided an approach for the bottom-up fabrication of two-dimensional (2D) nanostructures.[2] These systems represent a new class of functional materials, because unique properties or functions may arise from the unsaturated metal centers as well as from the molecular ligands.[3] A particularly attractive family of ligands are porphyrins with functional peripheral substituents, because the macrocyclic group of the porphyrin offers an additional coordination site for metal atoms and ions.[4]

The reaction of porphyrins and their artificial analogues, the phthalocyanines, with coadsorbed metal atoms has been studied for various metals such as Fe, Co, Ni, Cu, Zn, and Ce.[4d,5] According to a combined experimental and theoretical study of this complex reaction sequence,[5b] the metal atom (M) is first coordinated by the intact porphyrin, forming a metastable initial complex. This complex can undergo a thermally activated intramolecular redox reaction, by which the metal atom (M) is oxidized to its dication, while the pyrrolic hydrogen is released as H_2. As a result, the M(II) porphyrin complex is formed. The activation barrier for the redox reaction was predicted to increase in the order Fe < Co < Ni < Cu < Zn. Fe and Co were predicted to react already at room temperature, in agreement with the experiment, whereas Ni, Cu, and Zn require elevated temperatures.[5b]

Here, we report on the self-assembly and reaction of 5,10,15,20-tetra(4-pyridyl)porphyrin (2HTPyP, molecular structure shown in Figure 1e) with Cu on a Au(111) surface investigated by scanning tunneling microscopy (STM), X-ray

Received: January 18, 2012
Published: March 13, 2012

   dx.doi.org/10.1021/ja300593w | J. Am. Chem. Soc. 2012, 134, 6401−6408

photoelectron spectroscopy (XPS), and density functional theory (DFT) calculations. We have found that Cu reacts in two ways with 2HTPyP: (a) neutral Cu(0) atoms are coordinated by the peripheral pyridyl (py) substituent and link them to form a 2D coordination network; (b) Cu(0) is coordinated by the inner nitrogen atoms of the porphyrin macrocycle and, at elevated temperatures, oxidized to Cu(II) by an intramolecular redox reaction, which leads to the formation of the corresponding Cu(II) porphyrin complexes. This metalation follows a two-step mechanism: first, a Cu atom is attached to an intact macrocyclic pore forming an initial complex of Cu(0)−2HTPyP; in the second step, the macrocyclic pore is dehydrogenated while Cu is oxidized to Cu(II), which forms a copper(II) tetrapyridylporphyrin (CuTPyP) complex with the dehydrogenated porphyrin ligand, in agreement with previous work.[5b] Furthermore, we found that the annealing treatment promotes the metalation process, whereas the coordination in the linking position is only enhanced by annealing below ∼500 K. At higher temperatures, the network turns into a close-packed structure of CuTPyP, while the Cu atoms released from the bridging positions alloy with the Au substrate. This study demonstrates a dual functionality of the porphyrin ligand, resulting in the formation of a mixed-valence two-dimensional (2D) coordination network with alternating Cu(0) and Cu(II) centers. This potentially bifunctional network structure represents a 2D analogue of a 3D mixed-valence metal−organic framework (MOF).[6]

2. EXPERIMENTAL AND COMPUTATIONAL DETAILS

The experiments were conducted in two ultrahigh-vacuum systems. For the XPS experiments, a Scienta ESCA 200 photoelectron spectrometer with a monochromatized Al Kα X-ray source was used. The base pressure was in the low 10^{-10} mbar range. Photoelectrons were detected under 70° relative to the surface normal, in order to achieve higher surface sensitivity. For deconvolution of the spectra by means of least-mean squares fits, a Voigt-type peak shape was approximated by a weighted sum of Gaussian and Lorentzian functions (pseudo-Voigt function). A maximum number of restrictions was applied in order to increase the significance of the fit with respect to the interpretation given in the text, even if this resulted in reduced numerical agreement between fit and experimental data. In particular, the peak intensity ratios between the different nitrogen species and between nitrogen and Cu species were strictly coupled to the molecular stoichiometries. In addition, we used fixed peak separations between iminic and pyrrolic N in 2HTPyP (from previous XPS studies of 2HTPP on Au)[7] and in the initial complex Cu(0)−2HTPyP (from data of 2HTPP on Cu(111)).[7] This approach strictly limits the number of variables (with one remaining variable being the ratio between unreacted 2HTPyP and the initial complex) and thus makes the fit much less arbitrary than it may seem. Slight variations of the peak position (up to 0.1 eV) have statistical reasons. The STM experiments were conducted in an ultrahigh-vacuum system (Omicron Nanotechnology) with base pressure below 5×10^{-10} mbar. A tungsten tip was used, and all STM measurements were performed in a constant-current mode. The STM data were processed with WSxM software.[8]

For sample preparation, the 5,10,15,20-tetra(4-pyridyl)porphyrin (Sigma-Aldrich) molecules were deposited at a source temperature of 650 K by physical vapor deposition (PVD) onto a single-crystal Au(111) surface held at room temperature. Copper was deposited sequentially with molecule evaporation using an electron-beam evaporator. Note that the initial Cu dosage always exceeded the amount needed for full metalation and coordination, as evidenced by the presence of Cu islands in the STM images and the Cu(0) signal in the XP spectra. After deposition of both reactants at room temperature, postannealing treatments at different temperatures were applied as indicated in the text, and the samples were characterized *in situ* by STM and XPS at room temperature. Coverages are given in ML; 1 ML corresponds to one adsorbate atom or molecule per substrate surface atom. In contrast, the expression "one monolayer" describes a complete molecular layer, that is, the maximum number of molecules in direct contact with the surface within a close-packed layer. One monolayer corresponds to 0.035 ML, according to STM.

All DFT calculations were performed using local GGA (OLYP[9]) and hybrid GGA (B3LYP, BP3W91[9a,10]) functions using the 6-31G(d)[11] and 6-311+G(d,p) basis sets. Stationary points were confirmed to be minima or transition states by calculating the normal vibrations within the harmonic approximation. All DFT-computed relative energies are corrected for zero-point vibrational energies (ZPE). We used different levels of theory because it is not clear *a priori*[12] which combination of density functional and basis set is appropriate for treating metalloporphyrin systems.

3. RESULTS

For the STM and XPS investigations, we prepared samples using two different deposition sequences. In sequence I, 2HTPyP was deposited first onto Au(111), and Cu deposition followed. The order of deposition was reversed in sequence II.

3.1. Coordination Reactions at Room Temperature. Deposition of 2HTPyP onto Au(111) at 300 K leads to the formation of self-assembled close-packed monolayer domains involving weak intermolecular van der Waals or hydrogen bonding interactions (see Figure S1, Supporting Information). A similar behavior was reported previously for 2HTPyP on Ag(111).[5c] Following deposition sequence I, ∼0.1 ML of Cu was deposited onto the adsorbed 2HTPyP molecules (∼0.4 monolayer or 0.014 ML, see section 2 for the definition of the coverage units used here). This leads to the formation of islands with rhomb-shape network structures, as shown in the corresponding STM image (Figure 1a). Since this network structure emerges exclusively upon the co-deposition of Cu, one can conclude that it must involve Cu atoms. Our previous study[13] confirmed that these islands are typical of 2D metal−organic coordination networks stabilized by py−Cu−py coordination. The bottom part (green square) of Figure 1a shows an area of a close-packed molecular monolayer phase, indicating that the 2HTPyP molecules in this area are not coordinated by Cu. For comparison, Figure1b shows an STM topograph of a sequence II sample. In contrast to the sequence I sample, here islands of the coordination network are the predominant structure and the close-packed molecular phase is rarely observed. It is worthwhile to note that most of the surface area that is not occupied by the network appears very noisy in the STM scanning and shows a "gray" contrast (cf. area marked by "G" in Figure 1b), while the narrow regions between two nearby network islands appear stable and dark (cf. area marked by "D" in Figure 1b). This phenomenon implies the existence of freely moving 2D gas molecules on the surface. These 2D gas molecules move too fast to be imaged steadily by STM and thus give rise to the "gray" noisy signal. In contrast, in those narrow regions there are very few moving molecules, so the regions appear dark and stable in the STM images.

The difference between the two sample preparation sequences can be attributed to their different growth kinetics: On the sequence I sample, before the Cu deposition, some of the 2HTPyP molecules formed the close-packed molecular structure whereas others were in the 2D gas phase. The two phases were in a thermodynamic equilibrium governed by the sample temperature and intermolecular interactions. As Cu

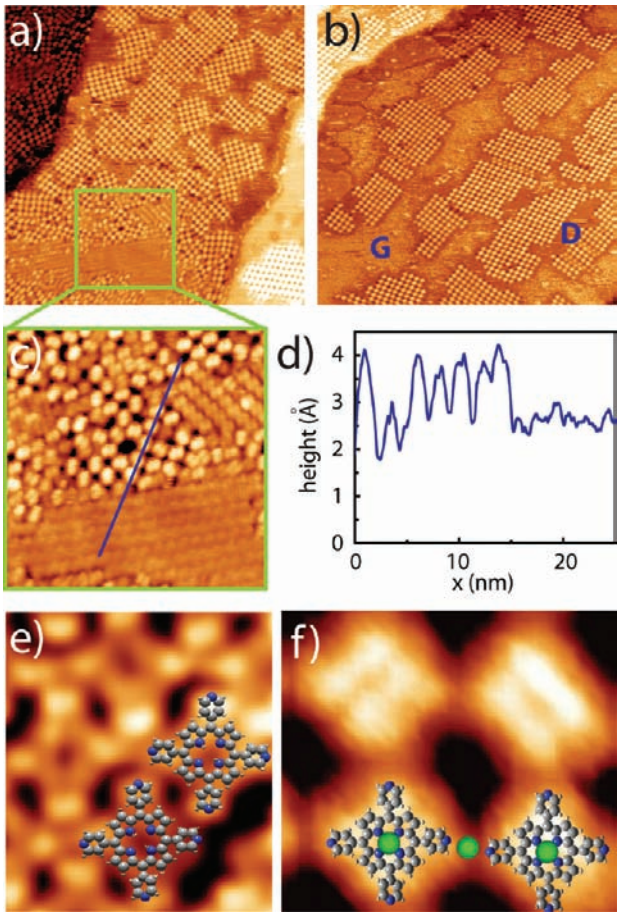

Figure 1. STM topograph of 2HTPyP with Cu deposited onto a Au(111) surface at 300 K. (a) 2HTPyP deposited first and Cu followed (100 × 100 nm^2, −1.28 V, 0.22 nA). (b) Cu deposited first and 2HTPyP followed (100 × 100 nm^2, −1.31 V, 0.28 nA). (c) A magnified view (30 × 30 nm^2, −1.28 V, 0.22 nA) of panel a. (d) Profile of the blue line in panel c from top to bottom. (e, f) High-resolution images (4.5 × 5 nm^2, −0.79 V, 0.29 nA) showing submolecular features with molecular models of 2HTPyP nitrogen in blue and carbon in gray) and Cu atoms overlaid; green refers to Cu(0). Cu coverage ≈ 0.1 ML; 2HTPyP coverage ≈ 0.4 monolayer or 0.014 ML.

atoms were deposited onto the surface, they coordinated with the 2D gas molecules forming the network structure coexisting with the preformed close-packed molecular phase. As revealed in Figure 1a, the network domains enclose the close-packed molecular layer, which hinder the dissolution of the latter into the 2D gas phase. On the sequence II sample, while the 2HTPyP molecules were deposited onto the surface, they had a certain probability to encounter the preadsorbed Cu atoms directly to form the coordination networks; consequently, the close-packed molecular phase is not as abundant as on the sequence I sample.

Figure 1c is a magnified view of the coexisting network phase and molecular phase of the sequence I sample. (TPyP molecules are partially coordinated in the disordered phases, that is, one, two, or three of their four pyridyl groups are involved in py−Cu−py coordination.) Interestingly, the molecules of the network phase appear "brighter" than those of the densely packed molecular phase. To highlight the contrast diversity explicitly, a line profile is plotted in Figure 1d showing that the average topographic height of the molecules of the network phase is 4.0 Å while the height of the molecular phase molecules is 2.5 Å. Note that the height difference is obvious also in Figure 1b; that is, the network molecules appear bright, while the freely moving molecules appear dimmer as manifested by the "gray" contrast.

Besides the height difference, the two species exhibit different intramolecular features. Figure 1e,f shows STM images of the two phases with submolecular resolution. One can see that the molecules in the densely packed molecular phase show four lobes at the four pyridyl corners, while the molecules in the network phase show a two-lobe internal structure. The higher topographic appearance and the two-lobe intramolecular feature corroborate that this complex has structural and electronic characteristics that are very different from those of the intact 2HTPyP molecules. It is known that the different STM topographic characteristics may originate from different molecular conformation, different chemical states, or different adsorption configuration. In particular, it is known that metalated porphyrin molecules usually give rise to a different STM appearance. For example, the apparent height of FeTPyP is 0.7 Å larger compared with the 2HTPyP precursor; in addition, 2HTPyP exhibits a central depression and four protrusions at corners, while FeTPyP exhibits a central rod-like protrusion.[5c,14] We attribute the observed STM topographic diversity to the metalation of the porphyrin molecules with Cu: the molecules with the four corner lobe appearance and 2.5 Å height are intact 2HTPyP, while those with the two-lobe appearance (Figure 1f) and 4.0 Å height are associated with the formation of a metal complex between 2HTPyP and Cu. This attribution is further supported by the fact that such contrast and appearance diversity has never been observed in the absence of Cu; that is, the closed-packed molecular monolayer always exhibits a rather uniform height and appearance in STM (see Figure S1, Supporting Information).

To shed light onto the mechanism of the metalation reaction and to provide further evidence that the molecules with two-lobe appearance in Figure 1f are metal complexes, we have carried out XPS measurements. The bottom curve in Figure 2 shows the N 1s XP spectrum of a sample with only 2HTPyP on Au(111) (0.018 ML, equivalent to ∼50% of a complete monolayer). The three N species in 2HTPyP are resolved: two pyrrolic N atoms (−NH−, 399.4 eV, blue), two iminic N atoms (=N—, 397.4 eV, blue), and four N atoms in the peripheral pyridyl groups (Np, 398.3 eV, magenta). In the fit, the peak intensities I_{-NH-}, I_{Np}, $I_{=N-}$ have a fixed ratio of 2:4:2, to account for the molecular stoichiometry. The fixed peak separation between (−NH−) and (=N—) was taken from XPS data of tetraphenylporphyrin (2HTPP) on Au(111), where the peak positions can be precisely measured because no pyridyl-related peak is superimposed in that case.[7] This and all other fits of N 1s spectra here include one satellite peak (red line) to account for shakeup processes.

Deposition of 0.19 ML Cu at 300 K leads to substantial changes in the N 1s spectrum (second spectrum from bottom in Figure 2). All peaks related to 2HTPyP undergo a rigid shift by 0.6 eV toward higher binding energy, which is attributed to the work function decrease caused by Cu. According to a previous study, the work function decrease for the formation of a Cu−Au(111) surface alloy with ∼20% Cu is around 0.25 eV.[15] Since the shift observed here is 0.6 eV, there must be further contributions to the work function decrease, for example, the positive charging of the Cu atoms due to coordination (see section 3.3). This would cause a weakening

dx.doi.org/10.1021/ja300593w | J. Am. Chem. Soc. 2012, 134, 6401−6408

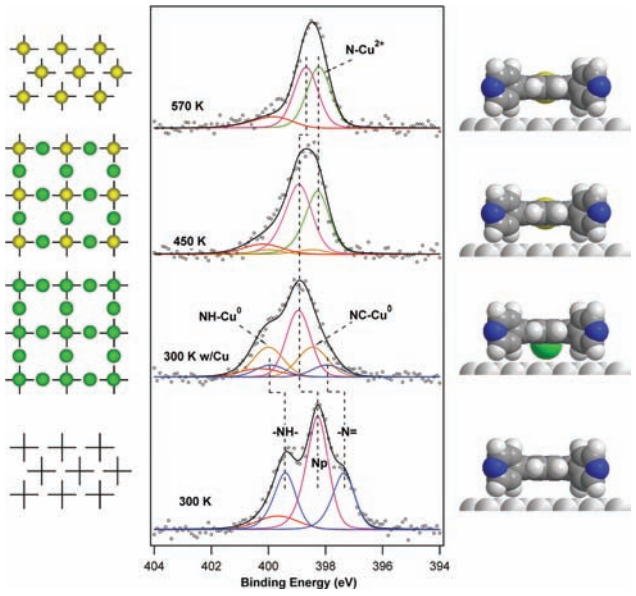

Figure 2. N 1s XP spectra of 2HTPyP on Au(111) (0.018 ML, ~50% of a monolayer) before (bottom) and after deposition of Cu atoms (0.19 ML) at 300 K and subsequent heating to the indicated temperatures (deposition sequence I). Line colors: blue refers to iminic and pyrrolic N of the porphyrin core in 2HTPyP; magenta refers to the pyridyl side groups; brown refers to iminic and pyrrolic nitrogen of the porphyrin core in the initial complex; green refers to CuTPyP; red refers to satellite features. The relative integrated intensities of the signals are (from bottom to top) 1, 0.75, 0.73, and 0.64; the reduction is due to the combined effects of damping by Cu and partial desorption. Note that the numerical agreement of the fit is limited by the tight constraints (see section 2). The models illustrate the corresponding idealized supramolecular (left) and molecular structures (right), according to STM; green refers to Cu(0) and yellow to Cu(II).

of the interfacial dipole and thus reduce the work function. The two additional peaks (brown, labeled as NH−Cu^0 and NC−Cu^0 at 400.0 and 398.4 eV, respectively) are attributed to the initial complex between 2HTPyP and Cu as imaged in Figure 1f. To account for the molecular stoichiometry (2:2), the two additional peaks have identical intensities. The existence of such complexes between a neutral metal atom and a porphyrin has been shown previously for the surface-confined reaction of Zn with 2HTPP.[5b] In the initial complex between 2HTPyP and Cu, the intact porphyrin molecule coordinates to a neutral Cu atom, mainly via the iminic N atoms, which accordingly show a larger peak shift than the pyrrolic N atoms relative to the peak positions in 2HTPyP. This interpretation is in line with the Cu 2p XPS data (see below) and the DFT results shown in section 3.3, in particular the N−Cu bond lengths in the initial complex **1**. The separation of the two peaks for the central N atoms in the initial complex (brown lines) agrees with N 1s data for 2HTPP on Cu(111), where the analogous initial complex is formed and where the two peaks are well separated due to the absence of the pyridyl-related contribution.[7] The peak of the four pyridyl nitrogens (margenta line) is broader compared with the bottom spectrum (fwhm 1.0 and 0.9 eV, respectively). This broadening perhaps reflects the fact that some of the pyridyl groups coordinate to Cu atoms.

A quantitative analysis of the XPS data shows that the initial complex Cu(0)−2HTPyP is more abundant at this stage (71%) than unreacted 2HTPyP (29%). A statistical analysis of STM data such as that presented in Figure 1a shows that the ratio between the molecules involved in the network phase and the molecular phase is approximately 33% ("darker" species) to 67% ("brighter" species). By comparison with the XPS analysis, we attribute the "brighter" molecular species in the network phase to the initial complex.

Figure 3 shows Cu $2p_{3/2}$ XP spectra for 0.19 ML Cu on Au(111) (bottom) and for 0.018 ML 2HTPyP followed by deposition of 0.19 ML Cu at 300 K (second from bottom). These conditions are the same as were used for the corresponding N 1s spectrum in Figure 2. Both Cu 2p spectra show only a single peak at 932.2 eV, that is, at a typical Cu(0) position. This result indicates that, at 300 K, the coordination network contains only Cu(0) in both the initial complex and the bridging positions. In the following, we will focus on the evolution of the chemical state of the complexes and of the network structure at elevated temperatures.

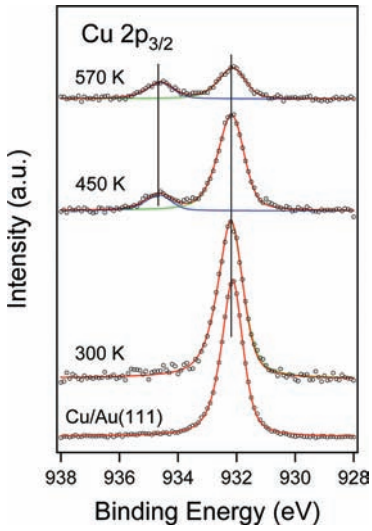

Figure 3. Cu $2p_{3/2}$ XP spectra of (from bottom to top) 0.19 ML Cu on Au(111) and 2HTPyP (0.018 ML, ~0.5 monolayers) on Au(111) after deposition of 0.19 ML Cu atoms at 300 K and after heating to elevated temperatures (450 K, 570 K). The peak at 932.2 eV is attributed to Cu(0); the peak at 934.7 eV is attributed to Cu(II) in CuTPyP, formed by direct metalation of 2HTPyP. The decrease of the Cu(0) signal is due to diffusion of Cu into the Au bulk.

3.2. Coordination Reactions at Elevated Temperatures. To investigate the temperature-dependent structural and chemical changes of the 2D coordination network, we annealed the samples in steps at increasing temperatures from 450 to 570 K. We found that both the sequence I and sequence II samples behaved similarly after the annealing (see Figures S2 and S3, Supporting Information), which confirms that the difference between the two sequences at 300 K (Figure 1a,b) is due to the kinetic effects. In detail, Figure 4a represents a typical STM topograph of a sequence II sample after a 450 K annealing step. Comparison with Figure 1a,b shows that after the annealing only network islands remain, while the molecular phase entirely disappeared. (Note that in the open area the scanning signal is very stable; that is, there is no such "gray" noise as appeared in Figure 1b, indicating that very few 2D gas molecules are present.) Hence, we conclude that annealing at 450 K transformed all molecules from the molecular phase into the network phase. This is possible because an excess of Cu (~3-fold) was provided initially. Another new feature is that

dx.doi.org/10.1021/ja300593w | J. Am. Chem. Soc. 2012, 134, 6401−6408

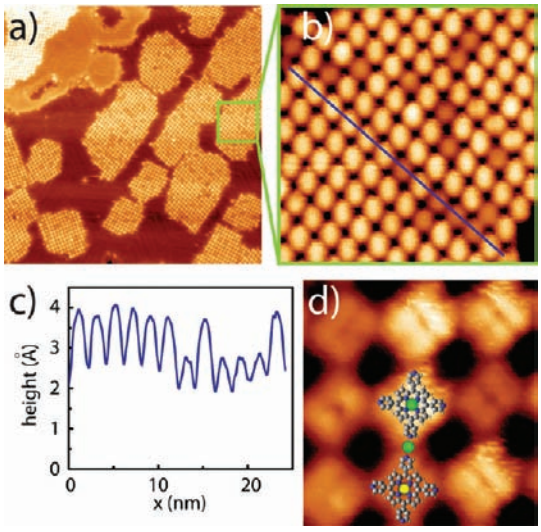

Figure 4. (a) STM topograph (150 × 150 nm^2, −1.31 V, 0.25 nA) of 2HTPyP with Cu deposited on a Au(111) surface after 450 K annealing (sequence II). (b) A magnified view (22 × 22 nm^2, −1.31 V, 0.25 nA) of panel a. (c) Profile of the blue line in panel b from top to bottom. (d) High-resolution image (7 nm ×6.5 nm^2, 1.21 V, 0.32 nA) showing intramolecular features with molecular models of TPyP and Cu atoms overlaid; yellow refers to Cu(II) and green to Cu(0).

some of the molecules within the network islands appear dimmer than others. Figure 4b is a magnified view showing this contrast difference. The line profile drawn in Figure 4c reveals that the height of the dimmer molecules is 2.8 Å, while the height of the brighter species is 4.0 Å. Figure 4d is a high-resolution STM image revealing that, despite the height difference, both the brighter and the dimmer molecules exhibit similar intramolecular features with two lobes. The dimmer molecules become more abundant after annealing the samples at higher temperatures (see below).

The N 1s XP spectrum acquired on the sequence I sample after annealing at 450 K for 2 min (third curve from bottom in Figure 2) is significantly narrower than the 300 K spectrum, because the contributions from the initial complex are strongly reduced. According to previous work,[5] the new peak at 398.3 eV (green) represents the central porphin nitrogen atoms of the fully metalated porphyrin species, Cu(II)TPyP (see below). According to a quantitative analysis, only 14% of the initial complex remains at this temperature. The peak related to the pyridyl N atoms (purple) has the same position as before heating.

The presence of Cu(II) after annealing at 450 K is proven by the Cu $2p_{3/2}$ XP data in Figure 3. The corresponding spectrum (third from bottom) shows a new peak at 934.7 eV, which is attributed to Cu(II) in Cu(II)TPyP. The position of the residual Cu(0) peak remains unchanged at 932.2 eV. The emerging of the fully metalated Cu(II)TPyP species as evidenced by the N 1s and Cu 2p XP spectra suggests that the dimmer molecules observed in STM (Figure 4) are indeed these Cu(II)TPyP complexes. Note that the number of the dimmer species in STM does not account for 86%. The discrepancy of the ratio of Cu(II) between STM and XPS may be due to statistical errors (both in XPS and STM) and possibly some differences in annealing temperature of STM and XPS experiments. Nevertheless, the observed trend that the dimmer species become more and more abundant with increasing temperature is consistent with this attribution.

Figure 5a shows an overview STM image of the sequence I sample after annealing at 520 K, and Figure 5b is a magnified

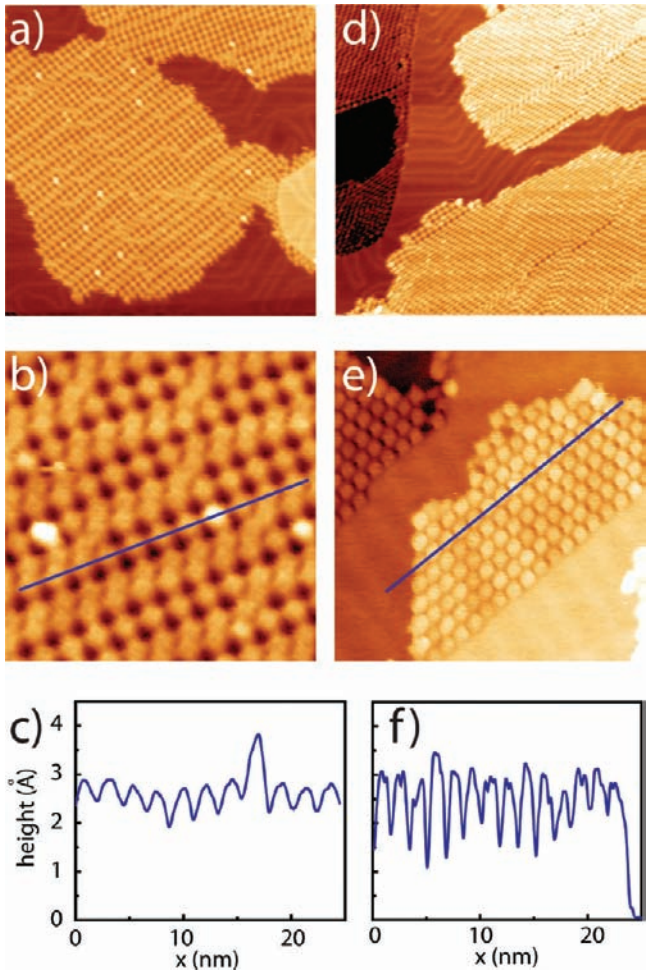

Figure 5. (a) STM topograph of 2HTPyP with Cu deposited onto a Au(111) surface (sequence II) after annealing at 520 K (100 × 100 nm^2, −1.11 V, 0.39 nA). (b) A magnified view of panel a (30 × 30 nm^2, −1.31 V, 0.28 nA). (c) Profile of the blue line in panel b from left to right. (d) STM topography of 2HTPyP with Cu deposited on a Au(111) surface (sequence I) after 570 K annealing (100 × 100 nm^2, −1.39 V, 0.46 nA). (e) A magnified view of panel d (25 × 25 nm, −1.39 V, 0.46 nA). (f) Profile of the blue line in (e) from top to bottom.

view. Both images reveal defect rows appearing in the network, which consist of closely packed molecules. The defect rows can be modeled as neighboring molecules being linked by weak (van der Waals or hydrogen bonding) intermolecular interactions. Most molecules exhibit a uniform height with few exceptions showing a pronounced height. The line profile drawn in Figure 5c indicates that the average height of the majority of molecules is 2.9 Å, while the higher one is 4.0 Å. After the samples are annealed at 570 K, the close-packed arrangement becomes more pronounced. Figure 5d shows that the molecules form very large domains of a close-packed structure, and no isolated network islands are observed. Only inside the close-packed domains or at the domain boundaries, small patches of the network structure remained. A similar transformation from the coordination network phase to the close-packed molecular phase was reported in Cu coordination with Zn(II)TPyP on Au(111).[16] This phenomenon was

dx.doi.org/10.1021/ja300593w | J. Am. Chem. Soc. 2012, 134, 6401−6408

tentatively attributed to Cu alloying with the Au substrate at high temperature, which results in Cu deficiency for coordination. The reduced intensity of the Cu $2p_{3/2}$ signal for 570 K in Figure 3 and the angle-dependent Cu $2p_{3/2}$ XP spectra in Figure S6 in the Supporting Information prove that this is indeed the case here (see also the separate discussion of the XPS data below): at 570 K, Cu atoms diffuse into the Au substrate, so Cu coordination is suppressed due to Cu deficiency; as a result, the arrangement of the molecules is dominated by weak intermolecular interactions. The molecules exhibit a very homogeneous topographic height of about 3.0 nm, as revealed by the magnified view in Figure 5e and the line profile in Figure 5f. Note that the apparent molecular height contrast in Figure 5e is due to the substrate herringbone reconstruction of the Au(111) surface.

The uniform molecular height suggests that the molecules are in a homogeneous chemical state and that virtually all 2HTPyP molecules reacted to form the complex Cu(II)TPyP. This is confirmed by the N 1s and Cu $2p_{3/2}$ XPS data. The N 1s spectrum taken after annealing to 570 K (top curve in Figure 2) shows only contributions from Cu(II)TPyP, while the signal components of the initial complex Cu(0)−2HTPyP disappeared. The pyridyl-related peak at 398.7 eV is shifted by 0.2 eV to lower binding energy relative to its position at 300 and 450 K but retains its width. This is in agreement with the observation derived from STM that the peripheral nitrogens lose their coordination with Cu: since the dative bonds N→Cu are removed, more electron density remains at the pyridyl-N, which should result in a lower N 1s binding energy. In the related Cu $2p_{3/2}$ spectrum (Figure 3, top curve), the component at 934.7 eV, attributed to Cu(II), increases by 5% relative to the 450 K spectrum, in agreement with the completion of the metalation reaction.

The intensity of the Cu(0) peak decreases when the sample temperature increases, while its position (932.2 eV) remains unchanged. The widths are 0.86 eV for Cu/Au(111) without porphyrin and 1.0 eV for the other spectra (with 2HTPyP). The fact that the width of the Cu(0) peak does not change between 300 and 573 K indicates that the different Cu(0) species (Cu in initial complex, Cu in bridging positions, Cu on or in the subsurface region of the Au surface) have essentially the same Cu $2p_{3/2}$ binding energy. At 573 K, only the latter Cu(0) species remains, because Cu atoms in the initial complex have already been oxidized to Cu(II), and the peripheral pyridyl groups no longer coordinate Cu(0) atoms, as can be seen in the STM images (Figure 5d,e). The decreasing overall intensity of the Cu $2p_{3/2}$ signal at elevated temperatures (Figure 3) and the angle-dependent Cu $2p_{3/2}$ XP data in the Figure S6, Supporting Information, prove that the Cu atoms thermally released from the py−Cu−py bridges diffuse to the subsurface and bulk region of the Au(111) sample.

Note that all XPS data presented here were taken using samples prepared with deposition sequence I. A parallel study with deposition sequence II yielded very similar results. The respective XPS data are presented in the Supporting Information (Figures S4 and S5).

3.3. Density Functional Theory (DFT) Calculations. To obtain a detailed mechanistic understanding of the metalation reaction, we performed gas-phase DFT calculations of the reaction between the porphyrin core (2H-porphyrin (2HP) was here used as the model system) and a Cu atom at different levels of theory along the lines of our previous publication on the mechanism of direct porphyrin metalation.[5b] Figure 6

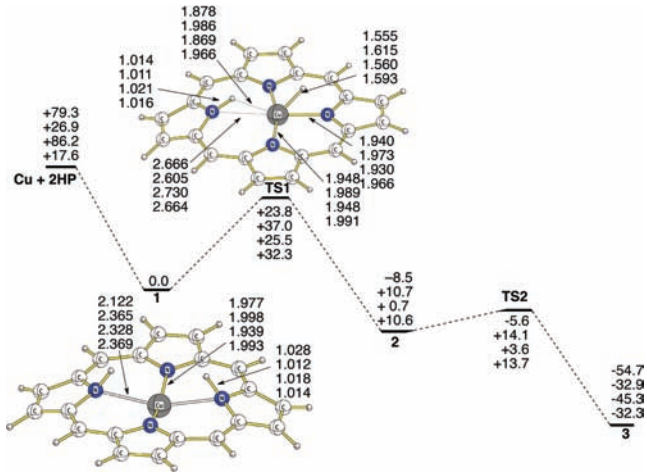

Figure 6. Schematic energy profile for the reactive insertion of a Cu atom into a porphyrin macrocycle in the gas phase: E + ZPE in kcal mol^{-1} at B3LYP/6-31G* (first entry), B3LYP/6-311+G** (second entry), OLYP/6-31G* (third entry), and OLYP/6-311+G** (fourth entry). Bond lengths are given in Å.

shows the lowest-energy reaction profile for the reaction of a bare Cu atom with 2HP at the different levels of theory. The first stage of the reaction is the barrierless formation of the initial complex **1**. This reaction is exothermic with respect to the ground-state Cu atom and 2HP at infinite separation by −79.3 and −86.2 kcal mol^{-1} at the B3LYP/6-31G* and OLYP/6-31G* levels of theory, respectively. Inclusion of the larger basis set (i.e., triple-ξ quality basis set 6-311+G**) lowers the exothermicity of the formation of the initial complex to −26.9 (B3LYP) and −17.9 kcal mol^{-1} (OLYP).

From the initial complex **1**, the reaction proceeds via the late transition state **TS1**, which describes a hydrogen transfer from the pyrrolic N to the Cu atom, to form the intermediate **2**. The formation of intermediate **2** is exothermic at all levels of theory. Transfer of the other pyrrolic hydrogen atoms to the Cu atom via the early transition state **TS2** and desorption of H_2 complete the reaction, the end product of which is the Cu(II) porphyrin, **3**. The first barrier is by far the largest with activation energies between 23.8 (B3LYP/6-31G*) and 37.0 kcal mol^{-1} (B3LYP/6-311+G**). Similar trends were found at the OLYP/6-31G* and OLYP/6-311+G** levels of theory (barriers for the **TS1** formation are 25.5 and 32.3 kcal mol^{-1}).

We also compared results of the calculations for 2HP with the results for the metalation of the larger 2HTPyP system at the B3LYP/6-31G* level. The barrier for the **TS1a** formation is then 32.3 kcal mol^{-1}, see Figure S7 in the Supporting Information. This means that the reactions will be sufficiently fast at the time scale of our experiment in the range between 400 and 600 K, if a pre-exponential Arrhenius factor of the order of 10^{13} s^{-1} is assumed, in agreement with our experimental observation. (Note that the comparability is limited by the fact that all influences of the substrate surface on the reaction are ignored in the calculation.)

In order to investigate the mechanism of the coordination of Cu atoms by the pyridyl groups, the DFT gas-phase calculations were extended to the larger CuTPyP model system. The formation of CuTPyP−Cu−CuTPyP (geometry optimization resulted in a linear N−Cu−N orientation with Cu between two pyridyl nitrogens, see Figure 7) was found to be exothermic by −85.3 kcal mol^{-1} (at the B3LYP/6-31G* level of

dx.doi.org/10.1021/ja300593w | J. Am. Chem. Soc. 2012, 134, 6401−6408

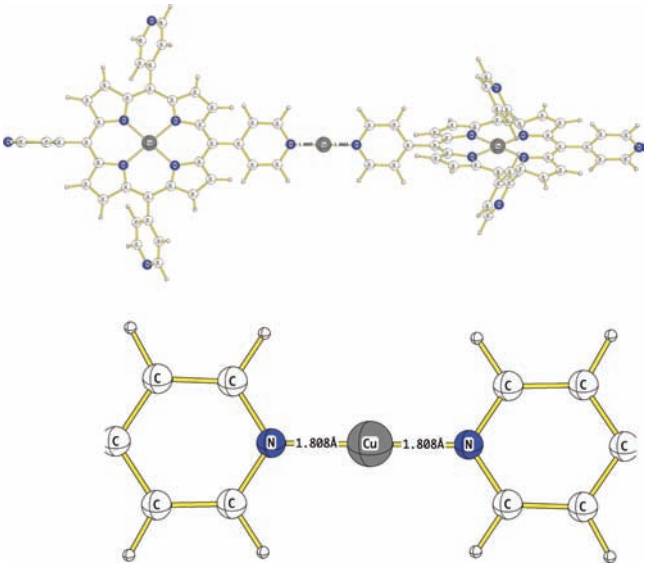

Figure 7. Geometry of the CuTPyP−Cu(0)−CuTPyP bridges, according to gas-phase DFT calculations. The geometry optimization resulted in a linear N−Cu−N orientation with Cu between two pyridyl nitrogens. The bottom part of the figure shows an enlarged view of the py−Cu−py bridge.

theory) and −91.3 kcal mol^{-1} (at the B3PW91/6-31G* level). The N−Cu bond length in the py−Cu−py bridge was found to be 1.81 and 1.82 Å at the B3PW91/6-31G* and B3LYP/6-31G* levels of theory, respectively. One should stress here again that calculations were performed without taking into account effects of the surface. Since the adsorbed Cu atom has the surface as an additional bonding partner, it is to be expected that the actual Cu−N bonds are weaker in the adsorbed state. This would explain why the calculated values suggest that the network is stable up to 650−700 K (as estimated using the Arrhenius equation with a pre-exponential of the order of 10^{13} s^{-1}), whereas the experiment shows that the py−Cu−py bonds are broken at much lower temperatures.

To gain insight into the oxidation state of Cu in the initial complex Cu−2HTPyP (**1a**), in the final complex CuTPyP (**3a**), and in the py−Cu−py bridge, a charge analysis (B3LYP/6-31G*, Mulliken and NBO)[17] was performed. In **1a**, the charge of the coordinated Cu atom was found to be +0.5e (+0.8e, NBO), while in the final complex **3a** a charge of +0.9e (+1.1e, NBO) was found. This result is in agreement with the Cu 2p XPS data, which show that the oxidation state of Cu in the final complex **3a** is higher than that in the initial complex **1a**. (Note that the computed real charges of coordinated metal ions are usually lower than the formal ion charges, due to covalent contributions to the coordinative bond and resulting electron donation from the ligand to the metal center.) In CuTPyP−Cu−CuTPyP, the charge for the Cu atom in the py−Cu−py bridge is +0.4e (+0.7e, NBO). This is only slightly lower than the charge for the Cu atom in the initial porphyrin complex and explains why the two species cannot be distinguished by their Cu 2p XPS signals.

4. CONCLUSIONS

We have shown that tetrapyridylporphyrin (2HTPyP) molecules on Au(111) exhibit a bifunctional behavior toward coadsorbed Cu atoms. On the one hand, the molecules coordinate neutral Cu(0) atoms with the N atoms in the peripheral pyridyl groups, such that one Cu atom links two pyridyl groups of neighboring molecules forming linear py−Cu−py bridges. This coordination process leads to the formation of a two-dimensional metal−organic coordination network at 300 K. On the other hand, Cu(0) is also coordinated by the four N atoms of the porphyrin macrocycle, which results at 300 K in the formation of a Cu(0)−2HTPyP complex. These initial complexes were identified by XPS and STM; DFT calculations predict that they are metastable, in agreement with previous experimental and theoretical investigations. At elevated temperatures (450 K), these Cu(0) complexes undergo an intramolecular redox reaction. As a result, the coordinated Cu atom is oxidized to a Cu(II) ion, which is fully incorporated into the porphyrin macrocycle, forming the complex Cu(II)TPyP. The network structure persists at this temperature. Thus, the bifunctional nature of the 2HTPyP molecules results, by reaction with Cu atoms, in a mixed-valence coordination network with alternating Cu(0) and Cu(II) centers. Considering the different reactivities of Cu(0) and Cu(II), this is a potentially bifunctional 2D metal−organic structure. At 570 K, the py−Cu−py coordination disappears, and the Cu(II)TPyP complexes form a densely packed molecular monolayer structure. The Cu(0) atoms released from the py−Cu−py coordination diffuse into the Au(111) substrate. Gas-phase DFT calculations show that coordination of Cu(0) by the intact porphyrin is energetically favorable and that the formation of the final CuTPyP complex has an activation barrier of 24−37 kcal mol^{-1}, depending on the method used. Formation of the py−Cu−py bridges was also found to proceed exothermically (85−91 kcal mol^{-1}) and to result in a linear N−Cu−N geometry.

■ ASSOCIATED CONTENT

Ⓢ Supporting Information

STM data of close-packed 2HTPyP layer, sequence I sample after 420 K annealing and sequence II sample after 570 K annealing, N 1s and Cu $2p_{3/2}$ XP spectra for deposition sequence II, angle-dependent Cu $2p_{3/2}$ XP spectra, DFT results for the metalation of 2HTPyP, and Gaussian Archive entries and absolute energies for all computed species. This material is available free of charge via the Internet at http://pubs.acs.org.

■ AUTHOR INFORMATION

Corresponding Author

michael.gottfried@chemie.uni-marburg.de; phnlin@ust.hk

Notes

The authors declare no competing financial interest.

■ ACKNOWLEDGMENTS

This work is financially supported by Hong Kong RGC under Grant No. 602409, by the German Science Foundation (DFG) through Sonderforschungsbereich 583, by the Cluster of Excellence "Engineering of Advanced Materials", by the Interdisciplinary Center for Molecular Materials (ICMM), and by a grant of computer time on the Höchstleistungsrechner in Bayern II (HLRB II). J.X. thanks the Alexander von Humboldt Foundation for a Feodor Lynen Fellowship.

■ REFERENCES

(1) (a) Lehn, J.-M. *Supramolecular Chemistry: Concepts and Perspectives*; Wiley VCH: Weinheim, Germany, 1995. (b) Lehn, J. M. *Chem. Soc. Rev.* **2007**, *36*, 151−160. (c) Dinolfo, P. H.; Hupp, J. T.

Chem. Mater. **2001**, *13*, 3113−3125. (d) Holliday, B. J.; Mirkin, C. A. *Angew. Chem., Int. Ed.* **2001**, *40*, 2022−2043. (e) Yaghi, O. M.; O'Keeffe, M.; Ockwig, N. W.; Chae, H. K.; Eddaoudi, M.; Kim, J. *Nature* **2003**, *423*, 705−714. (f) Kitagawa, S.; Kitaura, R.; Noro, S. *Angew. Chem., Int. Ed.* **2004**, *43*, 2334−2375.

(2) (a) De Feyter, S.; De Schryver, F. C. *Chem. Soc. Rev.* **2003**, *32*, 139−150. (b) Lin, N.; Stepanow, S.; Ruben, M.; Barth, J. V. *Top. Curr. Chem.* **2009**, *287*, 1−44. (c) Stepanow, S.; Lin, N.; Barth, J. V. *J. Phys.: Condens. Matter* **2008**, *20*, No. 184002. (d) Wan, L. J. *Acc. Chem. Res.* **2006**, *39*, 334−342.

(3) (a) Decker, R.; Schlickum, U.; Klappenberger, F.; Zoppellaro, G.; Klyatskaya, S.; Ruben, M.; Barth, J. V.; Brune, H. *Appl. Phys. Lett.* **2008**, *93*, No. 243102. (b) Gambardella, P.; Stepanow, S.; Dmitriev, A.; Honolka, J.; de Groot, F. M. F.; Lingenfelder, M.; Sen Gupta, S.; Sarma, D. D.; Bencok, P.; Stanescu, S.; Clair, S.; Pons, S.; Lin, N.; Seitsonen, A. P.; Brune, H.; Barth, J. V.; Kern, K. *Nat. Mater.* **2009**, *8*, 189−193. (c) Fabris, S.; Stepanow, S.; Lin, N.; Gambardella, P.; Dmitriev, A.; Honolka, J.; Baroni, S.; Kern, K. *Nano Lett.* **2011**, *11*, 5414.

(4) (a) Shi, Z. L.; Lin, N. *J. Am. Chem. Soc.* **2010**, *132*, 10756−10761. (b) Yokoyama, T.; Kamikado, T.; Yokoyama, S.; Mashiko, S. *J. Chem. Phys.* **2004**, *121*, 11993−11997. (c) Yoshimoto, S.; Yokoo, N.; Fukuda, T.; Kobayashi, N.; Itaya, K. *Chem. Commun.* **2006**, 500−502. (d) Gottfried, J. M.; Marbach, H. *Z. Phys. Chem.: Int. J. Res. Phys. Chem. Chem. Phys.* **2009**, *223*, 53−74. (e) Otsuki, J. *Coord. Chem. Rev.* **2010**, *254*, 2311−2341.

(5) (a) Gottfried, J. M.; Flechtner, K.; Kretschmann, A.; Lukasczyk, T.; Steinrück, H.-P. *J. Am. Chem. Soc.* **2006**, *128*, 5644−5645. (b) Shubina, T. E.; Marbach, H.; Flechtner, K.; Kretschmann, A.; Jux, N.; Buchner, F.; Steinrück, H.-P.; Clark, T.; Gottfried, J. M. *J. Am. Chem. Soc.* **2007**, *129*, 9476−9483. (c) Auwärter, W.; Weber-Bargioni, A.; Brink, S.; Riemann, A.; Schiffrin, A.; Ruben, M.; Barth, J. V. *ChemPhysChem* **2007**, *8*, 250−254. (d) Buchner, F.; Schwald, V.; Comanici, K.; Steinrück, H.-P.; Marbach, H. *ChemPhysChem* **2007**, *8*, 241−243. (e) Buchner, F.; Flechtner, K.; Bai, Y.; Zillner, E.; Kellner, I.; Steinrück, H.-P.; Marbach, H.; Gottfried, J. M. *J. Phys. Chem. C* **2008**, *112*, 15458−15465. (f) Bai, Y.; Buchner, F.; Wendahl, M. T.; Kellner, I.; Bayer, A.; Steinrück, H.-P.; Marbach, H.; Gottfried, J. M. *J. Phys. Chem. C* **2008**, *112*, 6087−6092. (g) Écija, D.; Trelka, M.; Urban, C.; de Mendoza, P.; Mateo-Martí, E.; Rogero, C.; Martín-Gago, J. A.; Echavarren, A. M.; Otero, R.; Gallego, J. M.; Mirandat, R. *J. Phys. Chem. C* **2008**, *112*, 8988−8994. (h) Auwärter, W.; Schiffrin, A.; Weber-Bargioni, A.; Pennec, Y.; Riemann, A.; Barth, J. V. *Int. J. Nanotechnol.* **2008**, *5*, 1171−1193. (i) Weber-Bargioni, A.; Reichert, J.; Seitsonen, A. P.; Auwärter, W.; Schiffrin, A.; Barth, J. V. *J. Phys. Chem. C* **2008**, *112*, 3453−3455. (j) Chen, M.; Feng, X. F.; Zhang, L.; Ju, H. X.; Xu, Q.; Zhu, J. F.; Gottfried, J. M.; Ibrahim, K.; Qian, H. J.; Wang, J. O. *J. Phys. Chem. C* **2010**, *114*, 9908−9916. (k) Di Santo, G.; Castellarin-Cudia, C.; Fanetti, M.; Taleatu, B.; Borghetti, P.; Sangaletti, L.; Floreano, L.; Magnano, E.; Bondino, F.; Goldoni, A. *J. Phys. Chem. C* **2011**, *115*, 4155−4162. (l) Écija, D.; Auwärter, W.; Vijayaraghavan, S.; Seufert, K.; Bischoff, F.; Tashiro, K.; Barth, J. V. *Angew. Chem., Int. Ed.* **2011**, *50*, 3872−3877.

(6) Férey, G.; Millange, F.; Morcrette, M.; Serre, C.; Doublet, M. L.; Grenèche, J. M.; Tarascon, J. M. *Angew. Chem., Int. Ed.* **2007**, *46*, 3259−3263.

(7) Buchner, F.; Xiao, J.; Zillner, E.; Chen, M.; Röckert, M.; Ditze, S.; Stark, M.; Steinrück, H.-P.; Gottfried, J. M.; Marbach, H. *J. Phys. Chem. C* **2011**, *115*, 24172−24177.

(8) Horcas, I.; Fernández, R.; Gómez-Rodríguez, J. M.; Colchero, J.; Gómez-Herrero, J.; Baro, A. M. *Rev. Sci. Instrum.* **2007**, *78*, 013705.

(9) (a) Lee, C. T.; Yang, W. T.; Parr, R. G. *Phys. Rev. B* **1988**, *37*, 785−789. (b) Miehlich, B.; Savin, A.; Stoll, H.; Preuss, H. *Chem. Phys. Lett.* **1989**, *157*, 200−206. (c) Handy, N. C.; Cohen, A. J. *Mol. Phys.* **2001**, *99*, 403−412.

(10) (a) Becke, A. D. In *The Challenge of d and f Electrons: Theory and Computation*; Salahub, D. R., Zerner, M. C., Eds.; American Chemical Society: Washington DC, 1989, p 165; (b) Vosko, S. H.; Wilk, L.; Nusair, M. *Can. J. Phys.* **1980**, *58*, 1200−1211. (c) Becke, A. D. *J. Chem. Phys.* **1993**, *98*, 5648−5652.

(11) (a) Binning, R. C.; Curtiss, L. A. *J. Comput. Chem.* **1990**, *11*, 1206−1216. (b) Blaudeau, J. P.; McGrath, M. P.; Curtiss, L. A.; Radom, L. *J. Chem. Phys.* **1997**, *107*, 5016−5021. (c) Ditchfield, R.; Hehre, W. J.; Pople, J. A. *J. Chem. Phys.* **1971**, *54*, 724−728. (d) Francl, M. M.; Pietro, W. J.; Hehre, W. J.; Binkley, J. S.; Gordon, M. S.; DeFrees, D. J.; Pople, J. A. *J. Chem. Phys.* **1982**, *77*, 3654−3665. (e) Frisch, M. J.; Pople, J. A.; Binkley, J. S. *J. Chem. Phys.* **1984**, *80*, 3265−3269. (f) Gordon, M. S. *Chem. Phys. Lett.* **1980**, *76*, 163−168. (g) Hariharan, P. C.; Pople, J. A. *Theor. Chim. Acta* **1973**, *28*, 213−222. (h) Hariharana, P. C.; Poplea, J. A. *Mol. Phys.* **1974**, *27*, 209−214. (i) Hehre, W. J.; Ditchfield, R.; Pople, J. A. *J. Chem. Phys.* **1972**, *56*, 2257−2261. (j) Rassolov, V. A.; Pople, J. A.; Ratner, M. A.; Windus, T. L. *J. Chem. Phys.* **1998**, *109*, 1223−1229. (k) Rassolov, V. A.; Ratner, M. A.; Pople, J. A.; Redfern, P. C.; Curtiss, L. A. *J. Comput. Chem.* **2001**, *22*, 976−984.

(12) (a) Liao, M. S.; Watts, J. D.; Huang, M. J. *J. Comput. Chem.* **2006**, *27*, 1577−1592. (b) Liao, M. S.; Watts, J. D.; Huang, M. J. *J. Phys. Chem. A* **2005**, *109*, 7988−8000. (c) Shubina, T. E.; Clark, T. *J. Coord. Chem.* **2010**, *63*, 2854−2867. (d) Shubina, T. E. *Advances in Inorganic Chemistry*; 2010; Vol. *62*, Chapter 7, ISBN: 9780123808745.

(13) (a) Shi, Z. L.; Lin, T.; Liu, J.; Liu, P. N.; Lin, N. *CrystEngComm* **2011**, *13*, 5532−5534. (b) Li, Y.; Lin, N. *Phys. Rev. B* **2011**, *84*, 125418.

(14) Zotti, L. A.; Teobaldi, G.; Hofer, W. A.; Auwärter, W.; Weber-Bargioni, A.; Barth, J. V. *Surf. Sci.* **2007**, *601*, 2409−2414.

(15) Fain, S. C. Jr.; McDavid, J. M. *Phys. Rev. B* **1976**, *13* (4), 1853−1854.

(16) Shi, Z. L.; Lin, N. *ChemPhysChem* **2010**, *11*, 97−100.

(17) Foster, J. P.; Weinhold, F. *J. Am. Chem. Soc.* **1980**, *102*, 7211−7218.